The Influence of Secondary Flow Structures in a Turbocharger Turbine Housing in Steady State and Pulsating Flow Conditions

S. P. Lee, M. L. Jupp
Turbocharger Research Institute
University of Huddersfield
Huddersfield, United Kingdom
e-mail: Sam.lee@hud.ac.uk

A. K. Nickson
BorgWarner Turbo Systems
Bradford, United Kingdom

***Abstract*—This paper presents a computational investigation into the effect of volute secondary flow structures on turbine inlet flow conditions. The steady state results show Dean type vortices exist early in the volute. As a result a substantial variation in absolute flow angle at the volute exit was observed. Pulsed flow simulations showed that the size and position of the secondary flow structures are time dependent. The resulting volute exit flow conditions were also found to be time dependent with the absolute flow angle at the volute exit varying with pulse pressure. This paper shows that the secondary flow structures that exist in the volute as a result of cross sectional shape can have significant downstream effects on rotor performance.**

Keywords–turbine performance; volute flow; CFD, secondary flow.

I. INTRODUCTION

Environmental issues have, over recent years, become increasingly important. Government legislation has aimed to reduce emissions in many industries. This is of particular importance in the automotive sector, as it is estimated that light duty vehicles contribute approximately 15%, and heavy duty vehicles approximately 6%, to the EU's total CO_2 emissions [1].

In an effort to reduce emissions, turbocharging has become a desirable option, not only in diesel powered engines, but increasingly in gasoline engines too. The main aim of turbocharging is to improve performance and efficiency over a wide range of operation by utilizing waste energy in the exhaust gas.

Automotive turbochargers almost exclusively employ the use of radial flow turbines to drive the compressor stage. Radial turbines incorporate a volute to accelerate and direct exhaust gas flow into the rotor. Improved knowledge of the complex three-dimensional flow present in the volute can help to optimize rotor entry flow conditions to reduce losses and improve stage efficiency.

Volute design is driven by the ratio of the cross sectional area to the radius of the volute passage center (A/r ratio). The A/r ratio controls the rotor inlet flow angle and usually varies linearly around the volute passage [2] [3]. This relationship is based on one-dimensional, incompressible and free vortex flow. Work by [3] showed that the incompressible approach results in a volute with larger A/r's than those obtained when compressibility is accounted for. Furthermore, work by [4] found significant variations in free vortex predictions and experimental results. [4] showed significant circumferential non-uniformity in flow angles around the volute exit. Similar results were also noted by [5] and [6]. However, the one-dimensional, free vortex and incompressible design approach is still widely used in volute design.

Once the volute A/r has been set the volute cross sectional shape can be specified. This is usually a trade-off between performance and installation requirements with installation limits usually dominating [7].

There are a limited number of published investigations describing volute secondary flows and their impact on rotor inlet conditions. [8] used a 3D Navier Stokes solver coupled with the higher Reynolds Number k-ε turbulence model to investigate flow with a circular cross section volute with an offset rotor inlet. This work presented both experimental and 3D CFD results that showed secondary flow structures becoming stronger between azimuth angles of 45deg and 270deg, as well as being stronger at the top and bottom of the volute cross section. Furthermore, low momentum energy was measured at the sharp corners around the volute exit, leading to high total pressure losses. [9] completed full stage CFD simulations and managed to capture detailed secondary flow structures within the volute. They showed that two counter rotating vortices formed within the trapezoid cross sectional shaped volute at approximately 90deg azimuth angle and continued to persist around the volute. Increased losses due to the existence of the secondary flow were found only around the end walls with the vortices positioned in the top corners of the volute.

Work by [7] looked further into the effect of volute cross sectional design on turbine performance. Two volutes with the same A/r but different volute aspect ratios (width/height) were tested. Volute A referred to a volute with an aspect ratio ranging from 0.8 near the tongue to 2.6 at the end of the volute passage whereas volute B had a constant aspect ratio of 1.7. From this study it was clear that a high entropy region was present at the shroud side of the blade inlet in both cases. The magnitude of the entropy increase was significantly larger in volute B as a result of the increased volute width. Distinct secondary flow patterns were also found in both volutes consisting of vortices of varying size. These vortex structures were much less distinct in volute A. The authors found that the difference in efficiency between

the two designs was not solely a result of efficiency gains in the volute but a significant improvement in rotor efficiency was also observed with volute A. The variation of the absolute flow angle around the volute exit circumference was found to vary between the designs with volute A showing more uniform flow especially under pulsating flow condition. It was also shown that the flow became increasingly non-uniform towards the shroud side of the volute exit, however only three points across the volute exit width (near the hub, midspan and near the shroud) were investigated.

Despite the insightful work by [7] the influence of cross sectional shape on secondary flow structures and rotor inlet conditions is still not fully understood. A better understanding of the development of secondary flows within turbine volutes and their influence on turbine inlet condition is vital knowledge to be incorporated into the volute design process.

The current paper describes the development of secondary flow structures within a circular cross section turbine volute under both steady state and pulsating inlet conditions. How such flow structures develop around the volute is investigated and the effect on turbine inlet conditions presented.

A. *Flow in Curved Pipes*

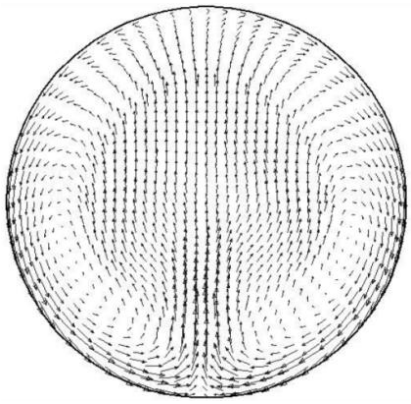

Figure 1 - Counter rotating dean vortices [10]

[10] investigated the effect of the upstream geometry on volute flow. The authors found that a curved manifold results in significant secondary flow structures. These secondary flow structures consist primarily of Dean Vortices which are a typical feature found in curved pipe flows [11] and [12]. Dean observed that vortices are created due to the velocity profile that exists over a pipe section, the lower speed flows at the boundaries have a correspondingly lower inertia. As a result when the flow encounters a bend the boundary flow moves radially inwards with a higher velocity than the higher inertia central flow. Thus two counter rotating "D" shaped vortices are formed as shown in Fig. 1. The strength of such secondary flow structures is expressed by the Dean number given in equation 1.

$$\boldsymbol{De = \sqrt{\frac{D}{R_C}}\, Re_D} \qquad (1)$$

where: De is the Dean Number, D is the pipe diameter, R_C is the radius of curvature and Re_D is the Reynolds number based on the pipe diameter.

Turbine volutes are a particularly interesting example of a curved pipe as both radius of curvature and diameter decrease with progression of azimuth angle. In addition to the complex geometry, a substantial pressure gradient exists driving the flow into the turbine rotor that has a significant impact on the volute flow.

II. COMPUTATIONAL SET-UP

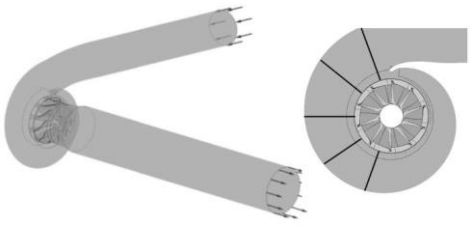

Figure 1. Full computational domain and 18°, 54°, 90°, 126° and 162° cross sectional plane positions in volute.

The computational domain and volute cross section are shown in Figure 2. The extended inlet and outlet regions are necessary to replicate the baseline experimental set up and to remove excess swirl causing recirculation at the outlet. A full domain specific mesh study was completed similar to that recommended by [13], this was extended to include a full boundary mesh independence study. The Y+ throughout the model was kept below 3. The volute mesh was highly refined with approximately 11 million cells to give good resolution of the volute flow. The inlet, volute and outlet regions were meshed using an unstructured tetrahedral mesh developed in ICEM CFD. The rotor region consists of a structured hexahedral mesh completed in ANSYS TurboGrid. The computational set-up was carefully validated against experimental gas stand testing. All CFD simulations were completed in CFX 14.5 using the Shear Stress Transport (SST) turbulence model, with the frozen rotor approach to account for the turbine rotation which was shown to be valid by [14]. The convergence criterion used was when the RMS residuals fell below $1e^{-4}$ and the efficiency values fluctuated by less than 0.05%.

III. RESULTS

A. *Steady State Analysis*

A significant variation in radial velocity was found over the volute cross section. Figure 3 shows streamlines and radial velocity contours at 18°, 54°, 90°, 126° and 162° from the volute tongue position as shown in Figure 2. These planes were selected to be positioned mid-way between the turbine rotor blades to minimize any upstream effect of the blade positions. At the 54° position, a complex flow structure is created as a result of a Dean-like effect. The significant pressure gradient acting to drive the flow into the wheel prevents a reversal of the central passage flow as per Dean vortices. The strong influence of this pressure gradient

means equation 1 does not solely govern the flow field. Instead, the combination of the Dean like effect and the pressure gradient, result in the rotor being fed from two volute flow regions; the near wall region with high radial velocity and the lower velocity central flow.

The vortices found to exist at the 54° are not present at any planes further around the volute. This is contrary to [9], where the secondary flow structure persisted throughout the volute, and the findings of [7] who found such structures up to the 270° plane. In the current study the cross section is of a circular shape and is symmetrical. As a result, the major secondary flow structures exist lower in the volute section compared with the trapezoidal shape tested by [9] where the vortices remained in the upper corners of the volute and hence were less effected by the strong radial pressure gradient into the wheel. It is thought that the reduction in volute cross sectional area with progression around the azimuth angle results in the pressure gradient influencing a larger proportion of the cross sectional area, therefore hindering secondary flow development beyond the first 90°. At the 90° plane, the streamlines at the volute exit show significant flow turning and a distinct ring of low radial velocity is present around the central flow. The effect of this is represented graphically in Figure 4 i), ii) and iii). In all cases, the data in the boundary layer regions have been removed. Figure 4 i) shows that at all positions, the maximum radial velocity into the rotor occurs towards the boundaries due to acceleration of flow around the volute walls. The minimum radial velocity at the rotor inlet was found at the plane center. The velocity components and absolute flow angle at the rotor inlet experienced their largest variation at the 90° and 126° positions. This is believed to be a result of the strong secondary flows present early in the volute migrating towards the rotor inlet, creating large variations in rotor inlet flow. At the 90° position, the absolute flow angle varies between 66° and 23.5° and at 126° the variation is 63° to 23.5°. It seems that while the strong secondary flow structures are positioned lower in the volute cross section, they degraded quickly with azimuth angle as a result of the strong pressure gradient and reducing volute cross sectional area. However, their low position results in significant effects on the rotor inlet conditions. While the variation in absolute flow angle is large at the 90° and 126° positions, at the 162° position the velocities and flow angle variation reduces showing a similar variation to that at the 54° position. This result remains almost constant around the remainder of the volute azimuth angle due to lack of secondary flow structures at later positions in the volute.

The absolute flow angles around the circumference of the volute exit are presented Fig. 4. The absolute flow angle is defined as the angle the flow makes with the blade LE in the absolute frame of reference. The absolute flow angle data is plotted at three axial positions, close to hub, midspan and close to shroud. The midspan absolute flow angles were found to be the most uniform of the three positions investigated. Both the hub and shroud absolute flow angles experience greater non-uniformity. Where [7] found the greatest non-uniformity near the shroud, in the current study, due to the symmetry of the volute cross section and symmetrical flow structures both the hub and shroud flow angles see similar variation. A drop in flow angle is observed early in the volute as a result of the tongue at all three positions. At the midspan section, the absolute flow angle then increases to an almost constant value over the remainder of the circumference. However, near the hub and shroud a second dip in flow angle is found just after the 90° position, at this position the radial velocity was found to experience the greatest variation as a result of the secondary flows. After the 180° position the absolute flow angle both near to the hub and shroud steadily increases as the volute cross section reduces and flow exiting the volute becomes increasingly uniform. Furthermore, the absolute flow angles across both the hub and shroud contours are substantially smaller than that present at the midpoint, this is a result of the velocity profiles across the volute exit width presented in Figure 4 i) and ii).

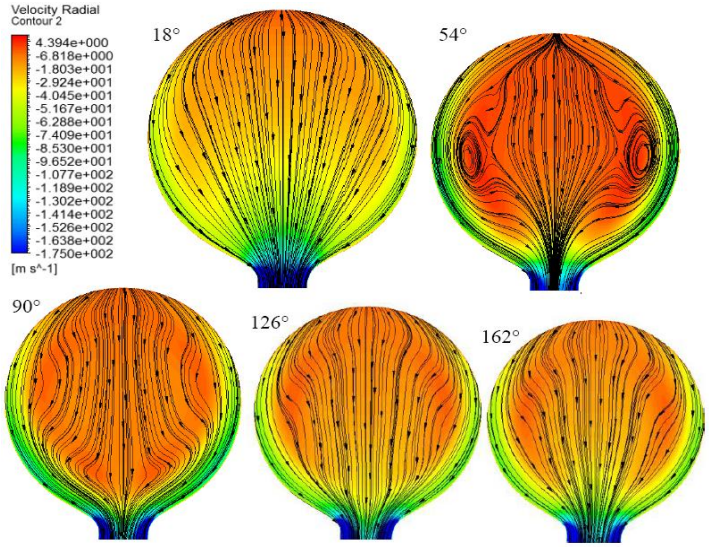

Figure 2. Radial velocity contours and streamlines plotted at 18°, 54°, 90°, 126° and 162° positions from top left to bottom right respectively peak efficiency running point.

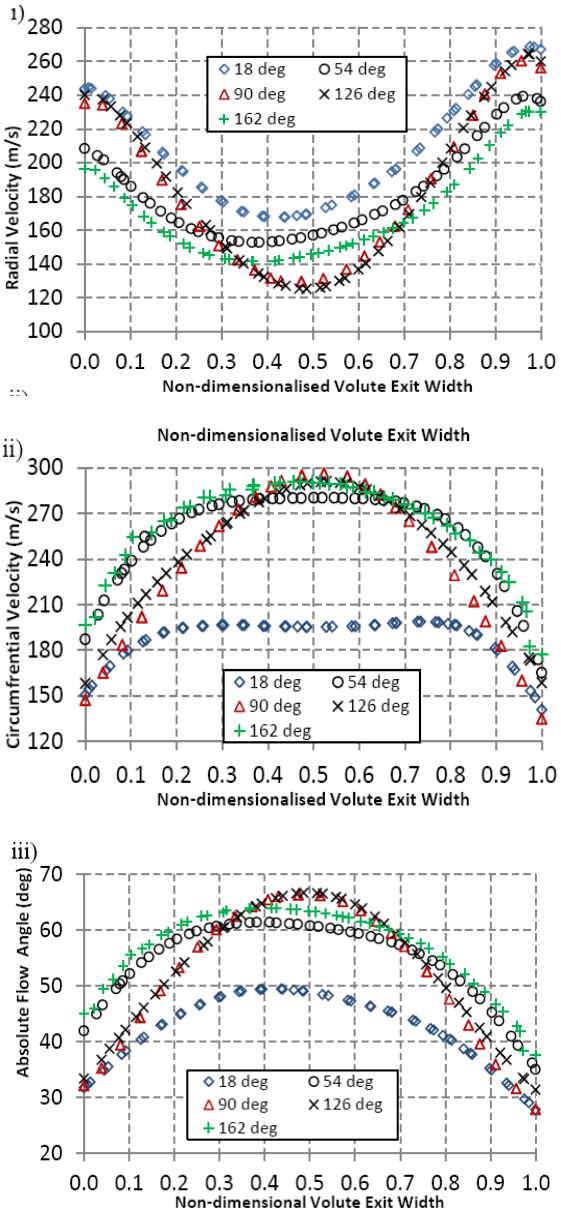

Figure 3. i) Radial velocity at volute exit 18°, 54°, 90°, 126° and 162° positions. ii) Circumferential velocity at volute exit at 18°, 54°, 90°, 126° and 162° positions. iii) Absolute flow angle at volute exit at 18°, 54°, 90°, 126° and 162° positions.

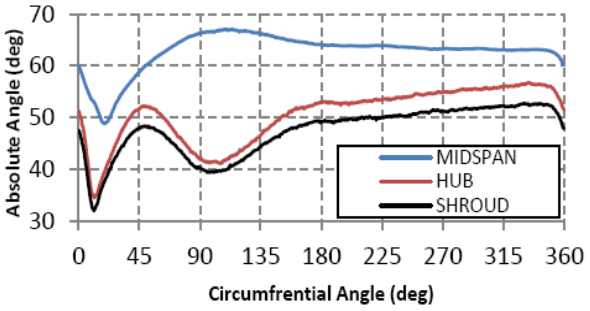

Figure 4. Absolute flow angles around the volute exit circumference at midspan, near the shroud and near the hub.

B. *Pulsed Flow Analysis*

In order to assess the effect of the secondary flow structures under pulsating conditions, the CFD simulations were extended to account for the pulsating nature of the exhaust flow. The exhaust pulses were modeled using a sinusoidal function to vary the total pressure at the inlet, while this method does not exactly replicate the shape of the exhaust pulse it is sufficient to model the hysteresis in the volute flow and has been used by [15] and [[16]]. The total temperature varied in accordance with the isentropic relationship - $P_t^{1-\gamma}T_t^{\gamma} = Const$. The pulse frequency was set to 40Hz with the total inlet pressure varying between approximately 155KPa and 245KPa.

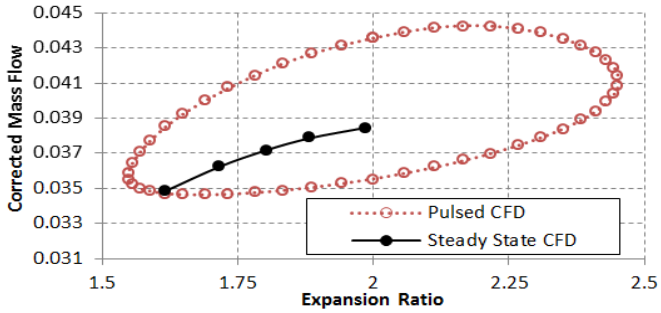

Figure 5. Steady state and pulsed flow mass flow parameter results.

Figure 6. Contour and streamline plots at the 54° position during the exhaust pulse. The graph (bottom right) shows the points in the pulse that the contour plots correspond to in order from the top left to bottom left.

The pulsed flow results are presented in Figure 6. The hysteresis loop formed in the pulsed flow case is a result of the periodic filling and emptying of the volute. This process occurs in a clockwise fashion with the increasing mass flow parameter the result of the volute filling and the reduction in mass flow occurring during the emptying process. The steady state data sits within the hysteresis loop.

Streamline and contour plots are shown in Figure 7 at the 54° position at points during the exhaust pulse. From Figure 7 it can be seen that the strength and position of the recirculation regions in the volute are time dependent. As the inlet pressure increases and the volute fills, the size of the recirculation reduces to a minimum as show at point B. During the volute emptying process, the size of the secondary flow structures increase from B to D. At position C, the recirculation regions appear smaller and slightly higher in the volute than found at points A and E, even though the inlet pressure is approximately equal. At the minimum point of the pulse, the vortices are largest and move down towards the volute exit as shown at point D. [17] found that for flow in curved pipes, as the Dean number increased, the core of the secondary flow moved towards the inner wall of the curve, similar to what is exhibited at position D. This indicates that at lower pressure ratios the Dean-like effect is more significant. At greater azimuth

angles qualitative analysis does not reveal the same time dependent effects that are observed at the 54° position.

The absolute flow angles at the volute exit at points during the pulse cycles are shown in Figure 8 at the 54°, 90° and 126° planes. It was observed that the minimum flow angle was obtained at point D where strong secondary flow structures were found low in the volute cross section. At points B and C the flow angles were greatest were the vortices were positioned higher in the volute. It was also shown that the greatest effect on the flow angle was achieved at the 90° and 126° position.

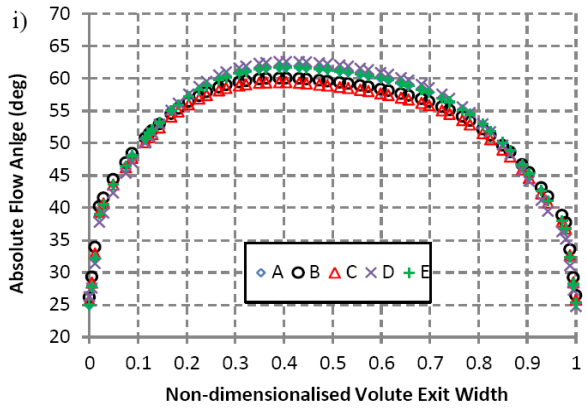

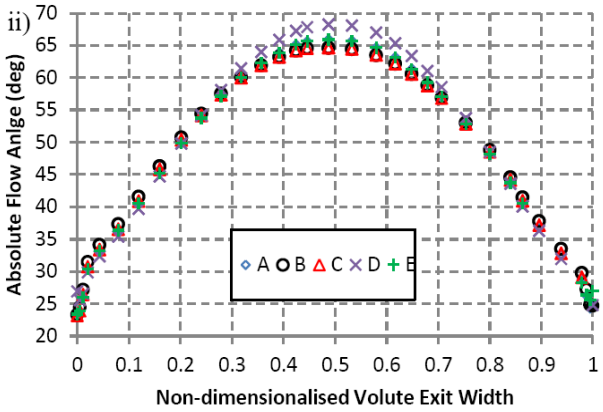

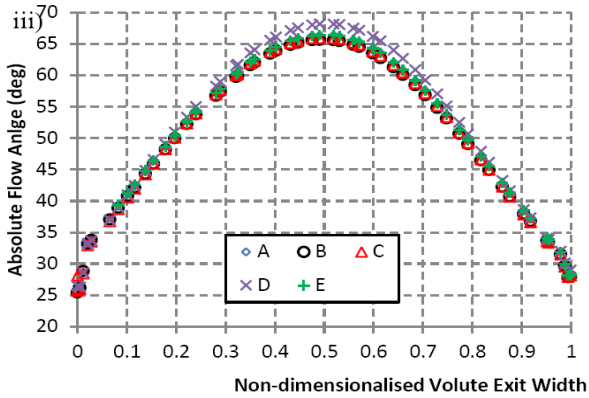

Figure 7. Absolute flow angle over the volute exit width at points A, B, C, D and E of the pulse as defined in figure 7. Graph i) data from 54° position, ii) 90° position and iii) the 126° position.

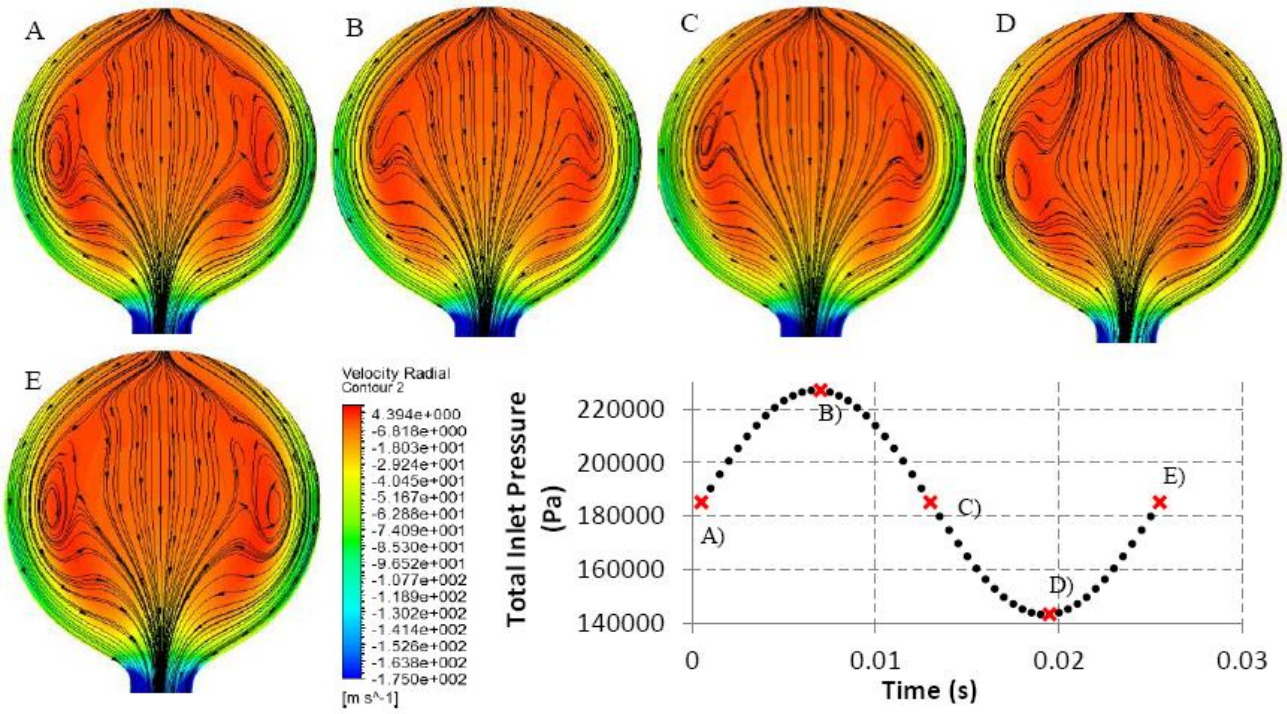

IV. CONCLUSION

This paper has shown how secondary flow structures develop in a circular cross sectional volute and the effect of such structures on the rotor inlet conditions. Both steady state and pulsed flow CFD simulation data has been presented. Significant secondary flow structures were found to exist in a circular cross sectioned volute but quickly degrade with progression around the azimuth.

Such secondary flow structures have a significant effect on the rotor inlet flow resulting in significant variation in rotor inlet flow angles. Under pulsed flow conditions, the secondary flow structures are time dependent. It was found that during the volute filling process secondary flow structures become weaker and sit higher in the volute. During the volute emptying the strength of the secondary flow increases and is focused lower in the volute causing larger a variation in the rotor inlet conditions.

Further work will be undertaken in order to validate the pulsed flow simulation data with pulsed gas stand testing. Furthermore a flow visualization technique will be implemented to validate the secondary flow structures observed in the simulation work.

ACKNOLEDGMENT

The authors would like to thank BorgWarner Turbo Systems for their support throughout this project.

NOMENCLATURE

De	Dean Number
D	Diameter
Re	Reynolds Number
R_C	Radius of Curvature
SST	Shear Stress Transport
RMS	Root Mean Squared
CFD	Computational Fluid Dynamics
P_t	Total Pressure
T_t	Total Temperature
γ	Ratio of Specific Heats
LE	Leading Edge
T-s	Total to static

REFERENCES

[1] European-Commission. Road Transport: Reducing CO2 emisions from vehicles. 2015.

[2] Chapple, P.M., P.F. Flynn, and J.M. Mulloy, *Aerodynamic Design of Fixed and Variable Geomtry Nozzleless Turbine Casings* Journal of Engineering for Power, 1980.

[3] Gu, F., A. Engeda, and E. Benisek, *A comparative study of incompressible and compressible design approaches of radial inflow turbine volutes.* Proceedings of the Institution of Mechanical Engineers, Part A: Journal of Power and Energy, 2001. 215(4): p. 475-486.

[4] Hussain, M. and F.S. Bhinder, *Experimental study of the performance of a nozzle0less volute casing for a turbocharger turbine.* SAE International, 1984.

[5] Scrimshaw, K.W., T., *Size Effects in Small Radial Turbines.* ASME, 1984.

[6] Benisek, E.S., W., *Laser Velocimeter Mesurements at the Rotor Inlet of a Turbocharger Radial Inflow Turbine* ASME, 1987. 55.

[7] Yang, M., et al., *Influence of Volute Cross-Sectional Shape of a Nozzleless Turbocharger Under Pulsating Flow Condition* ASME Turbo Expo, 2014.

[8] Martinez-Botas, R., K. Pullen, and F. Shi, *Numerical Calculations of a Turbine Volute Using a 3D Navier-Stokes Solver.* International Gas Turbine and Aeroengine Congress and Exhibition, ASME, 1996.

[9] Simpson, A.T., S. Spence, and J.K. Watterson, *A comparison of the flow structures and losses within vaned and vaneless stators for radial turbines.* Journal of turbomachinery, 2009.

[10] Hellstrom, F., *Numerical Computations of the Unsteady Pulsatile Flow in a Turbocharger*. 2010, KTH Mechanics.

[11] Dean, W.R., *Note on the Motion of Fluid in Curved Pipes.* Philosophical Magazine, 1927.

[12] Dean, W.R., *The Streamline Motion of Fluid in a Curved Pipe.* Philosophical Magazine, 1928.

[13] Galindo, J., et al., *Set-up Analysis and Optimisation of CFD Simulations for Radial Turbines.* Engineering Application of Computational Fluid Mechanics, 2014.

[14] Aymanns, R.S., J; Uhlmann, T; Luckmann, D, *A Revision of Quasi Steady State Modeling of Turbocharger Turbines in the Simulation of Pulse Charged Engines.* Aufladetechnische Konferenz Dresden, 2011.

[15] Galindo, J., et al., *Characterization of a radial turbocharger turbine in pulsating flow by means of CFD and its application to engine modeling.* Applied Energy, 2013. 103: p. 116-127.

[16] Zimmermann, R., et al., *Investigation on Pulsating Turbine Flow Radial Turbines.* Aachen Colloquium Automobile and Engine Technology, 2015.

[17] Greenspan, A.D., *Secondary Flows in Cruved Tubes.* Journal of Fluid Mechanics, 1973.